# Characterization of mixed CO2 + TBPB hydrates for refrigeration applications

P. Clain, Anthony Delahaye, L. Fournaison, S. Jerbi, N. Mayoufi, Didier Dalmazzone, Walter Fürst

*Proceedings of the 7th International Conference on Gas Hydrates (ICGH 2011), Edinburgh, Scotland, United Kingdom, July 17-21, 2011.*

# CHARACTERIZATION OF MIXED $CO_2$-TBPB HYDRATE FOR REFRIGERATION APPLICATIONS

**Pascal Clain*, Anthony Delahaye, Laurence Fournaison, Salem Jerbi**
**LGP2ES (EA21), Cemagref GPAN, 1 rue Pierre-Gilles de Gennes, CS 10030**
**92761 Antony cedex**
**FRANCE**

**Nadia Mayoufi, Didier Dalmazzone, Walter Fürst**
**ENSTA ParisTech, 75739 Paris cedex 15**
**FRANCE**

## ABSTRACT

The present work investigates the use of semiclathrate hydrates, formed from $CO_2$ + tetra-*n*-butylphosphonium bromide (TBPB) + water mixtures, as appropriate media for cold storage and distribution in refrigeration applications. Previous studies show that these hydrates are able to trap molecules of carbon dioxide resulting in mixed hydrates. Calorimetry devices were used for determining the dissociation enthalpies of mixed $CO_2$ + TBPB hydrates under various stability conditions (P, T) and salt concentrations. The results reveal that mixed $CO_2$ + TBPB hydrates can be considered as good candidates for air-conditioning, due to positive melting temperatures (between 282 to 289 K) at moderate $CO_2$ pressures (between 0.5 to 2 MPa). A hydrate solid fraction model was developed based on a $CO_2$ mass balance taking into account $CO_2$ solubility in aqueous tetrabutylphosphonium salt solution. The salt effect parameter was evaluated in order to estimate the influence of TBPB on the $CO_2$ solubility. Finally, in order to characterize the flow behavior of mixed $CO_2$ + TBPB hydrate slurries, a rheological study was carried out in a dynamic loop and an Ostwald-de Waele model was obtained.

*Keywords*: $CO_2$, TBPB, mixed hydrates, solubility, calorimetry, rheology, cold storage

## NOMENCLATURE

a Number of $CO_2$ molecules per unit hydrate structure
b Number of TBPB molecules per unit hydrate structure
c Number of $H_2O$ molecules per unit hydrate structure
D Pipe diameter [m]
k Consistency index [Pa.s]
L Length [m]
$m_{CO2,liq}$ Mass of $CO_2$ dissolved [kg]
$m_h$ Hydrate mass [kg]
$m_{liq}$ Aqueous solution mass [kg]
$\overline{M}_{H_2O}$ Molar mass of water [kg.mol$^{-1}$]
$\overline{M}_{TBPB}$ Molar mass of TBPB [kg.mol$^{-1}$]
$\overline{M}_h$ Molar mass of hydrate [kg.mol$^{-1}$]
n Behavior index
nh Quantity of hydrate [mol]
$n_{liq}$ Quantity of aqueous solution [mol]
$n^l_{CO_2}$ Quantity of $CO_2$ dissolved [mol]
Q Volume flow rate [m$^3$.s$^{-1}$]
R Pipe radius [m]
u Fluid velocity [m.s$^{-1}$]
$V_g$ Gas volume [m$^3$]
$V_{1iq}$ Liquid volume [m$^3$]

* Corresponding author: Phone: +33 (0)1 40 96 65 15 Fax +33 (0)1 40 96 60 75 E-mail: pascal.clain@cemagref.fr

$V_1$ Reservoir/Reference cell volume [$m^3$]
$V_2$ Measuring cell volume [$m^3$]
$x_s$ Mass solid rate of hydrate
$\rho_h$ Hydrate density [$kg.m^{-3}$]
$\rho_{liq}$ Aqueous solution density [$kg.m^{-3}$]
$\overline{\rho}_1^f$ Concentration of gas after dissolution in measuring cell [$mol.m^{-3}$]
$\overline{\rho}_2^i$ Concentration of gas before injection in reservoir cell [$mol.m^{-3}$]
$\overline{\rho}_2^f$ Concentration of gas after injection in reservoir cell [$mol.m^{-3}$]
$\Delta P$ Pressure drop [Pa]
$\dot{\gamma}_w$ Shear rate at the wall [$s^{-1}$]
$\phi_s$ Hydrate solid fraction [$m^3.m^{-3}$]
$\sigma_{CO_2}$ Solubility of $CO_2$ in aqueous solution [mol $CO_2.kg^{-1}H_2O$]
$\tau_0$ Minimal shear or yield stress [Pa]
$\tau_w$ Shear stress at the wall [Pa]
$\mu_{app}$ Apparent viscosity [Pa.s]

## INTRODUCTION

Secondary refrigeration is a method using a neutral fluid for cold distribution in order to confine primary refrigerants and reduce their quantities and thus their direct greenhouse effect due to gas emissions. Two-phase refrigerants (solid-liquid) are relevant for this method since their energy density is higher than a single phase secondary refrigerant thanks to the melting latent heat of the solid. Ice slurries are already used but their generation requires mechanical processes increasing exergy losses [1]. Hydrate slurries composed of a suspension of hydrate crystals in aqueous solution can also be used as secondary refrigerants and have the advantage of being able to be formed without mechanical processes. $CO_2$ hydrate can be a suitable possibility for secondary refrigeration applications because of its high dissociation enthalpy. As a result, $CO_2$ hydrate slurries can contain and carry large energy quantities [2-4]. However, the use of $CO_2$ hydrates in cooling systems is limited due to their formation pressure higher than 1 MPa. The addition of promoters, as quaternary salts or tetrahydrofuran (THF) is a solution to reduce the equilibrium pressure as shown in various studies [5-6]. Recently, among the quaternary salts, tetra-n-butylammonium bromide (TBAB) was particularly used for gas separation and cold transportation. TBAB hydrate can trap small gas molecule like $CH_4$ or $CO_2$ [7], and TBAB hydrate slurry was used as secondary refrigerant in various air-conditioning systems [8]. Previous rheological studies on clathrate hydrate slurries formed from aqueous solutions were carried out using a hydrate slurry loop and the capillary viscometer method [8-9]. Furthermore, gas dissolution can be enhanced in presence of quaternary salts in the aqueous solution. This property, known as salting-in effect [10-12], could increase hydrate formation rate.

In the present study, we report various experimental data and modeling results on $CO_2$-tetra-n-butylphosphonium bromide (TBPB) hydrate for a use in secondary refrigeration. First, we provide experimental data obtained by Differential Scanning Calorimetry (DSC) on the equilibrium conditions and the dissociation enthalpies of hydrates formed from $CO_2$ + TBPB + water mixtures. Since the available energy in hydrate slurries depends on the solid fraction, a model based on $CO_2$ balance was developed to determine hydrate fraction from pressure and temperature conditions. This model was validated by comparison with experimental data obtained in another calorimetric device (Differential Thermal Analysis, DTA), according to two different protocols of hydrate formation (by cooling or by gas injection). For modeling hydrate fraction, it is necessary to know $CO_2$ solubility in aqueous solution of TBPB. A characterization of $CO_2$ dissolution in a TBPB solution was thus carried out in the DTA device. Finally, an empirical model based on the capillary viscometer (Ostwald viscometer) method was applied to describe the rheological behavior of TBPB hydrate slurry flowing in a circulation loop. This empirical model is based on a Herschel-Bulkley-type equation integrating the solid fraction of the slurry.

## MATERIALS AND METHODS

### Differential Scanning Calorimetry and experimental protocol

The experimental setup used for the thermodynamic study is based on a high sensitivity differential scanning calorimeter, HP µDSCVII from SETARAM. This device measures continuously the exchanged heat flux between the sample cell and a thermostat during a predefined thermal program. As illustrated in DSC device

Figure 1, the HP µDSCVII is equipped with two pressure-controlled Hastelloy 0.25 $cm^3$ internal volume cells in which it is possible to work under pressures reaching 40 MPa. The DSC device can operate at a temperature between 228.15 and 393.15 K. The temperature and enthalpy calibration of the DSC in the range of 233 to 303 K was realized using the melting of high purity mercury and gallium samples. The sample cell was filled with approximately 50 µl of solution and then introduced into the calorimeter and connected to the gas feed line. After purging the sample cell with $CO_2$ to evacuate the air, $CO_2$ pressure was set to the desired value and kept constant during the experiments. For equilibrium point measurement, the same temperature program was repeated at increasing $CO_2$ pressures, from 0.5 to 2 MPa. It consisted of a cooling sequence down to 243.15 K at a rate of 2 K $min^{-1}$, an isotherm at 243.15 K for 20 min to allow sample crystallization, and a warming sequence up to 298.15 K at 0.5 K $min^{-1}$ to melt the solids. Warming thermograms were used for the determination of melting temperatures according to the protocol that has been described in detail [5]. For enthalpy measurements, the multi-cycle protocol described in previous works [13] was used to ensure the total conversion of the liquid phases to hydrates.

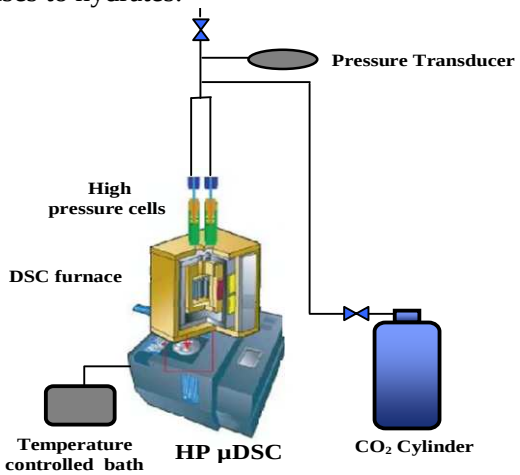


Figure 1 DSC device

**Differential Thermal Analysis and experimental protocol**

The DTA device was described in previous work [2]. It is illustrated in Figure 2. It is composed of two transparent test cells in polycarbonate of 30 mm internal diameter and a volume of 40.3 $cm^3$ and 41.5 $cm^3$, respectively for the measuring cell and the reference/reservoir cell. It is possible to work in the cells until 2.5 MPa and to study multiphase systems. A cooling/heating unit is used to regulate temperature in the system. Both cells are also equipped with pressure gauges. The principle of this calorimetric method consists in following heat flux between the studied sample and an inert reference material. By using several thermocouples in the cells, a very good temperature difference signal can be measured and recorded to obtain a DTA peak. This device is used to measure latent heat of transition or heat absorbed/produced by a medium.

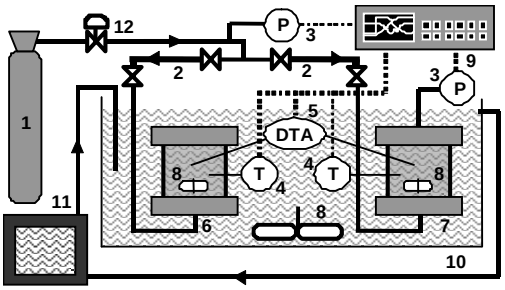


Figure 2 DTA device

1) $CO_2$ bottle 2) Injection pipe 3) Pressure gauge 4) Thermocouples 5) Differential Thermal Analysis 6) Reference/Reservoir cell 7) Measuring cell 8) Stirrers 9) Acquisition interface 10) Thermostatic bath 11) Cooling/heating unit 12) Pressure regulator

This DTA device was employed in our present work to study $CO_2$ dissolution in TBPB quaternary salt aqueous solution. For this purpose, the measuring cell is partially filled with 20 ml of salt aqueous solution, closed, degassed and the reservoir cell is filled with $CO_2$ without liquid solution. Both cells are then immerged into the thermostatic bath. After temperature stabilization in the cell, $CO_2$ is injected from the reservoir cell into the measuring cell. $CO_2$ injection takes one minute, during which valves allowing $CO_2$ access to the cell through the injection pipe are totally opened. After valves are closed, $CO_2$ dissolution equilibrium is considered reached when pressure inside the cell remains constant in time. This happens after about 2 hours from the end of the injection. Various temperatures are applied to the system which induces pressure change due to gas compression/expansion effect and gas dissolution in the solution. With a balance on $CO_2$, the quantity of gas dissolved in the aqueous solution is known:

$$n_{CO_2}^{l} = V_2\left(\overline{\rho}_2^{i} - \overline{\rho}_2^{f}\right) - \overline{\rho}_1^{f} V_g \qquad (1)$$

And the $CO_2$ dissolution is the ratio:

$$\sigma_{CO_2} = \frac{n^l_{CO_2}}{n_{liq}} \quad (2)$$

The behavior of two-phase fluids largely depends on solid fraction. Knowing this parameter is essential to control flowing conditions and determine the available energy quantity within the slurry. A model of hydrate solid fraction was explained in details in previous work [14]. The model is based on a mass balance on $CO_2$ in the various phases of the system: vapor phase, liquid phase, and hydrate phase. We assume a mixed hydrate composition from equilibrium data given in the literature [15]. This previous work provides the composition of a mixed TBPB-$CO_2$ hydrate in stoechiometric conditions using a Clausius-Clapeyron approximation. Finally, the model can be used to determine hydrate solid fraction from pressure, temperature, volume and gas quantity injected in the system. It was adjusted for our study:

$$n_h = \frac{n_{CO_2,\,tot} - \sigma_{CO_2} n_{\mathrm{liq}} - \bar{\rho}_1^f \left(V_1 - V_{liq}\right)}{1 - \left(\frac{c+b}{a}\right)\sigma_{CO_2} + \bar{\rho}_1^f \left( \frac{\frac{c}{a}\bar{M}_{H_20} + \frac{b}{a}\bar{M}_{\mathrm{TBPB}}}{\rho_{liq}} - \frac{\bar{M}_h}{\rho_h} \right)} \quad (3)$$

DTA device can also be used to experimentally evaluate hydrate solid fraction by enthalpy measurement. In fact, the ratio between heat measured by DTA during hydrate melting (kJ) and the theoretical latent heat of melting of hydrate ($kJ.kg^{-1}$) corresponds to hydrate mass:

$$m_h = \frac{DTA\ signal}{\Delta H_{melt}\, hydrate} \quad (4)$$

Hence, hydrate solid fraction obtained by DTA method is:

$$x_s = \frac{m_h}{m_{liq} + m_{CO_2,liq}} \quad (5)$$

Two different protocols for hydrate formation were tested. The first one consists in injecting gas continuously in a pre-cooled solution (opened system). The second one consists in cooling the system previously loaded with gas (closed system). Each protocol is performed under stirring condition until hydrate formation. After hydrate formation and stabilization, the system is dissociated by heating the cell .

**Experimental loop and experimental protocol**

The experimental loop illustrated in Figure 3 was described in a previous work [16]. It is composed of 316 L stainless steel pipes with an internal diameter of 8 mm and an external diameter of 10 mm, for a total inner volume of $2.97\ 10^{-4}\ m^3$. It is equipped with a 220-type Micro Pump (adjustable speed, differential pressure of 0.4 MPa, static pressure of 10 MPa), controlled by a Leroy Somer speed variator. A glass cylinder is used to control the visual aspect of the flow. The loop is equipped with 7 T-type thermocouples and two transducers (Sensit and Transinstrument, 0–5 MPa, precision 0.05%). All the sensors are connected to an acquisition system composed of an Agilent interface and a computer. The device is placed in an air-controlled room (1.68×0.85×2.10 m). A PID temperature-controlled system connected to a heating resistance and a refrigerating system was set up in order to apply temperature slopes and plateaus (accuracy: 0.4 K) to the circuit. The fluid flow is achieved by a 220-type Micro Pump. An electromagnetic flow meter (IFM6080K-type Variflux; maximum flow rate = 160 $l.h^{-1}$) is used to measure volumetric flow rate, while a differential pressure gauge is placed on a linear part of the circuit to measure pressure drops generated by the slurry.

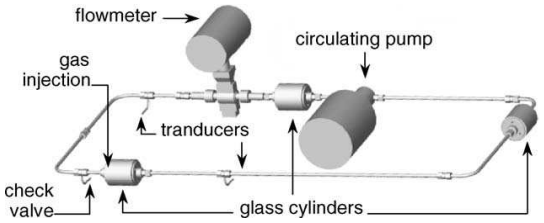


Figure 3 Experimental loop

The loop is loaded with an aqueous solution of TBPB flowing at an initial flow rate of 160 $l.h^{-1}$ and submitted to cooling in order to enable hydrate formation. During experiments, pressure, temperature and flow rate in the loop are recorded. The capillary viscometer method used to evaluate hydrate slurry rheology is based on various assumptions. In a first approximation, TBPB hydrate slurry can be considered as a pseudo-homogeneous fluid, circulating in laminar regime and without wall slip in the cylindrical pipe. Flow rate, shear stress, shear rate can thus be represented at the wall by the Rabinowitsch and Mooney's equation:

$$\frac{Q}{\pi R^3} = \frac{1}{4}\left(\frac{8u}{D}\right) = \frac{1}{\tau_w{}^3}\int_0^{\tau_w} \tau^2 \dot{\gamma}\, \mathrm{d}\tau \qquad (6)$$

Where $\tau_w$ is the shear stress at the wall, related to regular pressure drop $\Delta P$ due to a pipe of length $L$ and diameter $D$:

$$\tau_w = \frac{D\Delta P}{4L} \qquad (7)$$

After derivation of the expression of Rabinowitsch and Mooney, we solved a differential equation and obtained an expression of the shear rate at the wall:

$$\dot{\gamma}_w = \frac{8u(3n+1)}{D4n} \qquad (8)$$

Where $n$ is the behavior index defined as:

$$n = \frac{\mathrm{d}\ln\tau_w}{\mathrm{d}\ln\frac{8u}{D}} \qquad (9)$$

Thus, measurements of pressure drop $\Delta P$ and flow velocity $u$ allow the rheological behavior of the fluid to be established according to the Herschel-Bulkley's model:

$$\tau_w = \tau_0 + k \cdot \dot{\gamma}_w^n \qquad (10)$$

Finally, the apparent viscosity is defined as the ratio between the shear stress and the shear rate:

$$\mu_{app} = \frac{\tau_w}{\dot{\gamma}_w} \qquad (11)$$

## RESULTS AND DISCUSSION

### DSC device: Dissociations enthalpies of mixed $CO_2$-TBPB hydrate

Figure 4 represents thermograms for a TBPB solution with an initial mass concentration of 10% wt. This concentration of TBPB corresponds to the experimental conditions reported in the DTA sections. Stability conditions of mixed $CO_2$-TBPB hydrate are deduced from these thermograms according to the protocol described in details in previous work [12].

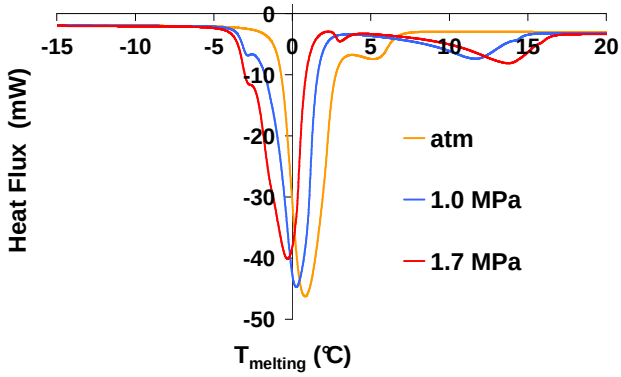


Figure 4 Thermogram for a 10% wt TBPB solution under various $CO_2$ pressure

The thermograms in Figure 4 show two peaks for each system. The first peak corresponds to a eutectic phase while the second one is only related to hydrate. Without gas (atm), the second peak corresponds to single TBPB hydrate melting. Under gas pressure, the second peak corresponds to a new phase composed of mixed $CO_2$-TBPB hydrate with a dissociation temperature higher than that of single TBPB hydrate and increasing with pressure. For the initial mass concentration of 10% wt, these measurements show that the melting temperature for mixed $CO_2$-TBPB hydrate is in a range between 278.3 and 286.8 K. Recent results by Mayoufi *et al.*[15] show that mixed TBPB + $CO_2$ hydrates have dissociation enthalpies close to that of ice and higher than that of single TBPB hydrate. The increasing of dissociation enthalpies and temperature is due to the addition of $CO_2$ which stabilizes the semiclathrate hydrate structure. The present DSC results at 10 wt% TBPB concentration are reported in another paper [17] at various TBPB concentrations and various $CO_2$ pressures. In the case of TBPB + $CO_2$ hydrate, the thermodynamic properties seem to be suitable for refrigeration applications as air-conditioning.

### DTA device: $CO_2$ dissolution

$CO_2$ dissolution was measured in salt aqueous solution of TBPB with a mass concentration of 10% wt at various temperatures. Figure 5 represents $CO_2$ solubility in a TBPB solution and compares this data with $CO_2$ solubility in pure water in the same temperature and pressure conditions that in the study of [18].

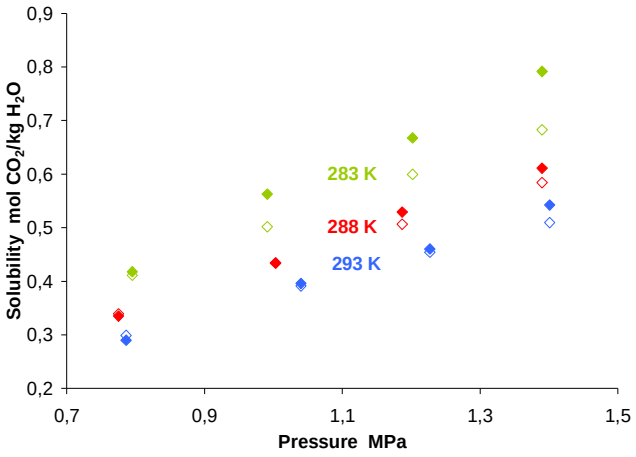


Figure 5 $CO_2$ dissolution in solution water + 10%wt TBTB. Solid shape denotes the $CO_2$ solubility in TBPB solution; open shape denotes $CO_2$ solubility in pure water

At constant temperature, $CO_2$ solubility increases with pressure because the gas is forced to dissolve in the solution. At constant pressure, $CO_2$ solubility decreases with temperature. This behavior is due to the partial molar enthalpy variation of solute which is negative (exothermic $CO_2$ dissolution) [19]. We notice that carbon dioxide dissolved more in a TBPB solution than in pure water: $CO_2$ is salted in. The salting-in effect can be explained by the interaction between electrolyte (gas, water) and non-electrolyte (salt). A theory based on Van der Waals forces explains salting-in effects of large ions such as quaternary salts. Desnoyers demonstrated that the dissolution of salts of large ions increases the quasi-crystalline structure of water, which decreases the entropy of the system hence increasing the solubility [20].

**DTA device: Solid hydrate fraction**

The characterization of $CO_2$ dissolution is used to calculate hydrate solid fraction based previous model [14]. Hydrate solid fraction was also estimated using a calorimetric method described by equation (4) in materials and methods section. Two different protocols were used to form hydrate in the measuring DTA cell: by gas injection and by cooling (see materials and methods). We note a good agreement between calorimetric method and solid fraction model, with a difference of 4.5 % and 3 % for gas injection and cooling methods respectively. The discrepancies are due to the assumption of thermodynamic equilibrium for the model. But during phase transitions, the system is not at the equilibrium. Furthermore, we suppose that the initial salt mass concentration remains constant during hydrate formation process. In fact, the salt fraction in the solution decreases as TBPB is consumed by hydrates. Hence, the final TBPB concentration is lower than initially. By taking into account this concentration decrease in the model, the accuracy of the results can be improved. Nevertheless, we can notice that the solid fraction obtained by gas injection is higher than that obtained by cooling. Indeed, the driving force related to hydrate crystal nucleation is different in both cases. In the first method, a mechanical force generates hydrate formation whereas in the second method, the driving force is thermal. Moreover, in the protocol by cooling, a hydrate crust appears at the gas-liquid interface in the beginning of crystallization, preventing the gas penetration in the aqueous solution and thereafter the entire hydrate formation process. With gas injection method, gas pressure breaks the crust and enables a higher dissolution.

| **Method** | **$P_{exp}$/MPa** | **$T_{exp}$/K** | **Latent heat DTA/ kJ** | **Theoretical latent heat /kJ.kg$^{-1}$water [15]** | **% Mass solid fraction** | |
|---|---|---|---|---|---|---|
| | | | | | DTA | Model |
| Gas injection | 1.39 | 278.3 | 1.1 | 397.7 | 24.4 | 25.5 |
| Cooling | 1.23 | 286.6 | 1.0 | 386.0 | 22.4 | 21.7 |

Tableau 1. Evaluation fraction solid

**Loop device: Flow properties of TBPB hydrate slurry**

We report data measurements to determine the rheological model for a TBPB hydrate slurry in a loop device equipped with a capillary viscometer. The device is loaded with an initial TBPB mass concentration of 15%wt. After pressure, temperature and flow stabilization, a sudden temperature raise occurs when hydrates appear, because hydrate crystallization is an exothermic phenomenon. In the same time, pressure drop also begins to increase since hydrate formation induces a higher apparent viscosity of the fluid. Hydrate slurry can be visualized in the glass cylinder: the transparent fluid becomes milky. Figure 6 represents the determination of the behavior index from experimental data. It could be approximated by a linear curve with a slope corresponding to *n*, the behavior index.

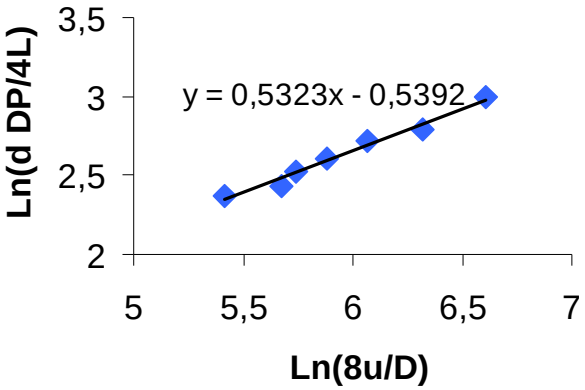


Figure 6 Determination of the behavior index for TBPB hydrate slurry with a volume solid hydrate fraction of 28.10%

The behavior index denotes the difference with a Newtonian behaviour. For an aqueous TBPB solution without hydrate, the behavior index is very close to 1 considered as the Newtonian behavior. Figure 7 represents the evolution of the behavior index of TBPB hydrate slurries for a hydrate volume fraction from 0 to 28%. The behavior index decreases linearly with the solid rate increasing.

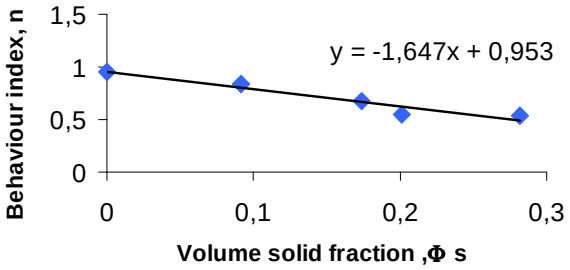


Figure 7 Evolution behaviour index in function of volume hydrate fraction

The TBPB hydrate slurry behavior index is lower than 1, which is related to a non-Newtonian behavior and a shear-thinning character. Thus, the apparent viscosity deduced from equation (11) decreases when the shear rate increases like most hydrate slurries in aqueous solution.

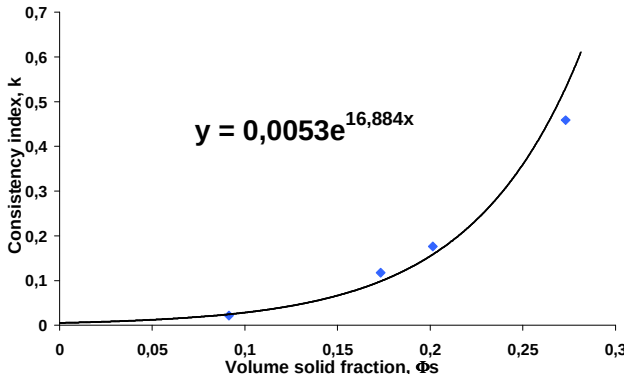


Figure 8 Evolution of consistency index with volume solid fraction

Figure 8 represents the evolution of the consistency index *k* as a function of TBPB hydrate volume fraction in the slurry. Firstly, this index is strictly inferior to 1 which means TBPB hydrate slurry behaves as shear-thinning fluid. Secondly, the consistency index increases exponentially when the volume solid fraction becomes higher than 15%vol, which means that the apparent viscosity will also increase significantly. In this range of solid fraction, experimental results show that yield stress is null. Thus, for TBPB hydrate slurry with a hydrate fraction between 9 to 28 %vol, the rheological behavior could be modeled by an Ostwald-de Waele's model:

$$\tau_w = k \cdot \dot{\gamma}_w^n \qquad (12)$$

$$\tau_w = 0.0053 \exp^{16.884\Phi_s} \cdot \dot{\gamma}_w^{-1.647\Phi_s + 0.953} \qquad (13)$$

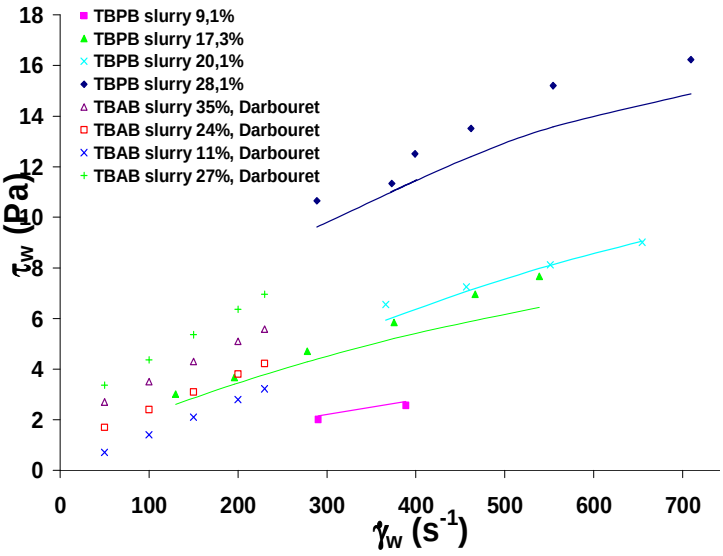


Figure 9 TBPB hydrate slurry rheograms for volume solid fraction from 9 to 28% (Points: experimental data; lines: model prediction; Open shapes: experimental data of Darbouret [9]).

Figure 9 represents experimental rheograms and results with Ostwald-de Waele's model for volume solid fraction from 9 to 28%. The agreement between experimental and model predictions is acceptable, but discrepancies appear at high volume fraction, especially for solid fraction of 28%vol. The rheological model depends mainly on the value of the consistency index. The correlation established for this index fits very well all the points except the one at 28%vol which is slightly below the tendency curve.

Our results are compared with the work of Darbouret [9] for TBAB hydrate slurry. Their study was carried out for shear rate up to 230 $s^{-1}$ and for volume solid fraction between 4 and 55 %. According to the authors, TBAB hydrate slurry behaves as a Bingham fluid, with a behavior index equal to 1 and a minimal shear stress different from zero. The rheograms for both quaternary salts are of the same order of magnitude with differences related to the different nature of salts. Moreover, the operating conditions are not similar in both studies and the measuring uncertainty (flow velocity, head loss, temperature) is not negligible. Also, the estimation of the solid fraction either by measuring or modeling induces important discrepancies between the models.

## CONCLUSIONS

Mixed $CO_2$-TBPB hydrates seem to be a good medium for refrigeration applications. Indeed, as shown in this study, the energy density of hydrates is close to that of ice, and their dissociation temperature is above 0°C, which is interesting for a use as phase-change material for cold storage. A comparison of two different methods of hydrate crystal formation using thermal analysis shows that direct gas injection in a pre-cooled solution increases the quantity of hydrate crystals formed in the system. Moreover, TBPB salted in carbon dioxide dissolution in aqueous solution, and thus improve hydrate formation. The rheological characterization of TBPB hydrate slurry in a dynamic loop shows a shear-thinning behavior for a solid fraction between 9 and 28%. Currently, a more detailed rheological study is in progress to complete the characterization of TBPB hydrate slurry flow properties, before studying mixed TBPB-$CO_2$ hydrate slurry.

## REFERENCES


[1] Guilpart J, Stamatiou E, Delahaye A, Fournaison L. *Comparison of the performance of different ice slurry types depending on the application temperature.* Int. J. Refrig. 2006;29:781-788.

[2] Fournaison L, Delahaye A, Chatti I, Petitet JP. *CO2 hydrates in refrigeration processes*. Industrial and Engineering Chemistry Research 2004;43(20):6521-6526.

[3] Marinhas S. *Caractérisation thermohydraulique de coulis d'hydrates de gaz en vue d'une application à la réfrigération secondaire*, Univ. of Université Paris 13 - Nord (2006).

[4] Marinhas S, Delahaye A, Fournaison L, Dalmazzone D, Furst W, Petitet JP. *Modelling of the available latent heat of a CO2 hydrate slurry in an experimental loop applied to secondary refrigeration*. Chemical Engineering and Processing: Process Intensification 2006;45(3):184-192.

[5] Delahaye A, Fournaison L, Marinhas S, Chatti I, Petitet JP, Dalmazzone D, Furst W. *Effect of THF on equilibrium pressure and dissociation enthalpy of CO 2 hydrates applied to secondary refrigeration*. Industrial and Engineering Chemistry Research 2006;45(1):391-397.

[6] Lin W, Delahaye A, Fournaison L. *Phase equilibrium and dissociation enthalpy for semi-clathrate hydrate of $CO_2$ + TBAB*. Fluid Phase Equilibria 2008;264(1-2):220-227.

[7] Shimada W, Ebinuma T, Oyama H, Kamata Y, Takeya S, Uchida T, Nagao J, Narita H. *Separation of Gas Molecule Using Tetra-n-butyl Ammonium Bromide Semi-Clathrate Hydrate Crystals*. Japanese Journal of Applied Physics 2003;42(Part 2, No. 2A):129-131.

[8] Fukushima S, Takao S, Ogoshi H, Ida H, Matsumoto S, Akiyama T, Otsuka T. *Development of high-density cold latent heat with clathrate hydrate*. NKK Technical Report 1999;166:65-70.

[9] Darbouret M, Cournil M, Herri J-M. *Rheological Study of TBAB Hydrate Slurries as Secondary Two-Phase Refrigerants*. International Journal of Refrigeration 2005;28:663-671.

[10] Bockris JOM, Bowler-Reed J, Kitchener JA. *The salting-in effect*. Transactions of Faraday society 1951:184-192.

[11] Pomaville RM, Poole SK, Davis LJ, Poole CF. *Solute--solvent interactions in tetra-n-butylphosphonium salts studied by gas*

*chromatography*. Journal of Chromatography A 1988;438:1-14.
[12] Sergeeva VF. *Salting-out and salting-in of non-electrolytes*. Russian Chemical Reviews 1965;34(4):309.
[13] Martinez MC, Dalmazzone D, Fürst W, Delahaye A, Fournaison L. *Thermodynamic properties of THF + $CO_2$ hydrates in relation with refrigeration applications*. AIChE Journal 2008;54(4):1088-1095.
[14] Marinhas S, Delahaye A, Fournaison L. *Solid fraction modelling for CO2 and CO2-THF hydrate slurries used as secondary refrigerants*. International Journal of Refrigeration 2007;30(5):758-766.
[15] Mayoufi N, Dalmazzone D, Fürst W, Delahaye A, Fournaison L. *CO2 Enclathration in Hydrates of Peralkyl-(Ammonium/Phosphonium) Salts: Stability Conditions and Dissociation Enthalpies*. Journal of Chemical & Engineering Data 2009;55(3):1271-1275.
[16] Delahaye A, Fournaison L, Marinhas S, Martínez MC. *Rheological study of CO2 hydrate slurry in a dynamic loop applied to secondary refrigeration*. Chemical Engineering Science 2008;63(13):3551-3559.
[17] Mayoufi N, Dalmazzone D, Delahaye A, Clain P, Fournaison L, Fürst W. *Experimental data on phase behavior of simple TBPB and mixed CO2 + TBPB semiclathrate hydrates*. Journal of Chemical & Engineering Data 2011:Submitted.
[18] Diamond LW, Akinfiev NN. *Solubility of CO2 in water from -1.5 to 100 °C and from 0.1 to 100 MPa: evaluation of literature data and thermodynamic modelling*. Fluid Phase Equilibria 2003;208(1-2):265-290.
[19] Battino R, Clever HL. *The solubility of gases in liquids*. Chemical Reviews 1966;(66):395-463.
[20] Desnoyers J, Perron G, Léger S, Okamoto B, Lilley T, Wood R. *Salting-in of alcohols in aqueous solutions by tetraalkylammonium bromides at the freezing temperature*. Journal of Solution Chemistry 1978;7(3):165-178.